Quantum Spectral Analysis by Continuous Measurement of Landau-Zener Transitions

Christopher C. Bounds,* Josh P. Duff, Alex Tritt, Hamish A. M. Taylor, George X. Coe, Sam J. White, and L. D. Turner

School of Physics and Astronomy, Monash University, Melbourne, Victoria 3800, Australia

(Received 6 June 2023; accepted 17 January 2024; published 27 February 2024)

We demonstrate the simultaneous estimation of signal frequency and amplitude by a single quantum sensor in a single experimental shot. Sweeping the qubit splitting linearly across a span of frequencies induces a nonadiabatic Landau-Zener transition as the qubit crosses resonance. The signal frequency determines the time of the transition, and the amplitude its extent. Continuous weak measurement of this unitary evolution informs a parameter estimator retrieving precision measurements of frequency and amplitude. Implemented on radio-frequency-dressed ultracold atoms read out by a Faraday spin-light interface, we sense a magnetic signal with estimated sensitivities to amplitude of 11 $\mathrm{pT}/\sqrt{\mathrm{Hz}}$, frequency 0.026 $\mathrm{Hz}/\mathrm{Hz}^{3/2}$, and phase 0.084 $\mathrm{rad}/\sqrt{\mathrm{Hz}}$, in a single 300 ms sweep from 7 to 13 kHz. The protocol realizes a swept-sine quantum spectrum analyzer, potentially sensing hundreds or thousands of channels with a single quantum sensor.

DOI: 10.1103/PhysRevLett.132.093401

The quest for ever more sensitive measurements, especially of signals emanating from micro- and nanoscale sources, leads inexorably to quantum sensors free from thermal noise and calibration drift [1]. Instruments that measure directly in the frequency domain—spectrum, signal, or wave analyzers—have been central to advances in physics, engineering [2] and speech science [3] amongst many other fields, for over a century [4,5]. A quantum spectrum analyzer is a quantum sensor measuring directly in the frequency domain, indicating both the amplitude and frequency of harmonic components within a frequency span. To date this has been realized by either incoherent noise spectroscopy [6] or coherent filter banks, where each measurement senses a distinct, fixed frequency. Continuous arrays of qubits formed by large ensembles in magnetic bias gradients have demonstrated multigigahertz spans but with intrinsic and inhomogeneous broadening limiting resolution to order 1 MHz [7,8]. Discrete arrays of qubits have the potential to achieve higher spectral resolution and sensitivity in reduced volume by using dynamical decoupling to render each qubit sensitive to a single frequency [9–18], harmonics series [19–22], or frequency band [23], and insensitive elsewhere. Analyzing a wide span at high resolution is a formidable scaling challenge for this approach, requiring many qubits with long coherence times, individually addressed for quantum control, and individually read out. To date such discrete filter banks have sensed four distinct frequencies [24]. In this Letter, we present an alternative approach to quantum spectrum analysis, with a spectral resolution equivalent to a filter bank with sixty channels, realized in a single-shot measurement of a single sensor under homogeneous control.

Instead of parallelizing across many qubits each sensing at a fixed frequency, we subject a single sensor comprising many atoms to time-dependent but spatially homogeneous control. We continuously sweep the sensing frequency of this single long-decoherence-time sensor across the span, while making a continuous weak measurement [25] of its unitary evolution. An unknown oscillating magnetic field within the frequency span induces a Landau-Zener transition between the diabatic eigenstates. Continuous measurement reveals the resonance time and hence signal frequency, while the deviation from the initial state encodes interaction strength and hence signal amplitude. Landau-Zener transitions are widely used in quantum control to generate rotations insensitive to shifts in resonance [26]. Here we show that Landau-Zener transitions open a new perspective on quantum measurement.

Our sensing qubit consists of Zeeman states dressed by resonant radio frequency radiation. The dressed state splitting is simply the Rabi frequency of this drive, and we realize the Landau-Zener spectrum analyzer by linearly increasing the drive amplitude over time. Dressed states have two important advantages for time-dependent sensing. First, dressing realizes continuous dynamical decoupling [10,11,15,16] from magnetic noise outside the span, including static detuning error and low-frequency technical noise. Second, the on-going Rabi flopping orthogonal to the Larmor precession enables a single-axis weak measurement to perform continuous state tomography [27] on the evolving dressed qubit.

The protocol can be understood by considering a spin-$\frac{1}{2}$ system with laboratory frame Hamiltonian $\hat{H}_0(t) = -\hbar\omega_{\mathrm{L}}\hat{\sigma}_{\mathrm{z}}/2 + \hbar\Omega_{\mathrm{c}}(t)\cos(\omega_{\mathrm{c}}t)\hat{\sigma}_{\mathrm{x}} + \hbar\Omega_{\mathrm{s}}\cos(\omega_{\mathrm{s}}t + \phi_{\mathrm{s}})\hat{\sigma}_{\mathrm{z}}$,

comprising constant Zeeman splitting ω_L, time-dependent control by resonant drive at radio frequency ω_c with swept amplitude $\Omega_c(t)$, and a weak test signal parameterized by amplitude Ω_s, oscillation frequency ω_s and phase ϕ_s. We increase the control amplitude at constant sweep rate λ, realizing the continuously varying Rabi frequency $\Omega_c(t) = \Omega_i + \lambda t$.

Transforming into the first rotating frame by $\hat{H}_{1I} = \hat{S}_1^\dagger \hat{H}_0(t)\hat{S}_1 - i\hbar\hat{S}_1^\dagger\hat{S}_1$ where $\hat{S}_1 = \exp(i\omega_c\hat{\sigma}_z t/2)$, and applying the rotating wave approximation (RWA) yields $\hat{H}_1 = (\hbar/2)[\Delta_c\hat{\sigma}_z + 2\Omega_s\cos(\omega_s t + \phi_s)\hat{\sigma}_z + \Omega_c(t)\hat{\sigma}_x]$. For convenience only, we now form $\hat{H}_{1R}$ by rotating $\hat{H}_1$ through $-\pi/2$ around $\hat{y}$ so that, in the absence of both control errors ($\Delta_c = 0$) and signal ($\Omega_s = 0$), the eigenstates are of $\hat{\sigma}_z$, and are split by $\Omega_c(t)$: this is our swept sensing qubit.

If we suppose for a moment that the signal frequency ω_s is known, we may transform to a second frame corotating at ω_s and make a second RWA yielding $\hat{H}_2 = (\hbar/2)[(\Omega_i + \lambda t - \omega_s)\hat{\sigma}_z + \Omega_s\cos(\phi_s)\hat{\sigma}_x - \Omega_s\sin(\phi_s)\hat{\sigma}_y]$. This is the canonical Landau-Zener Hamiltonian, merely with a delayed resonance time $t_{res} = (\omega_s - \Omega_i)/\lambda$, i.e., $\Omega_c(t_{res}) = \omega_s$. A signal of amplitude Ω_s induces an avoided crossing in the instantaneous eigenstates of $\hat{H}_2$, as seen in Fig. 1(a). A sweep that commences from a dressed eigenstate remains exponentially close to it until just prior to t_{res}. For a weak signal, and hence a small gap, the crossing is nonadiabatic and a partial transition to the other diabatic eigenstate occurs, manifest as a change in the longitudinal spin projection F_z^{1R} [Fig. 1(b), blue]. Henceforth we denote the time-dependent expectation value of spin projection on axis i by $F_i^P = F_i^P(t) = \langle\psi_P(t)|\hat{F}_i|\psi_P(t)\rangle$, where $|\psi_P(t)\rangle = c_+(t)|+_P\rangle + c_-(t)|-_P\rangle$ and $|\pm_P\rangle$ are the frame-P eigenstates. $\hat{F}_i$ are the atomic hyperfine spin-1 operators, and as described below, at all times $F_i = 2\langle\hat{\sigma}_i\rangle$. Under a nonadiabatic transition through the avoided crossing, a clear amplitude drop in the oscillating transverse projection F_y^{1R} is evident in Fig. 1(c). Minimizing total residual $\|F_{z,\mathrm{meas}}^{1R}(t) - F_z^{1R}(t, \omega_s, \Omega_s, \phi_s)\|_2$ between the continuously measured spin projection and the Bloch equations solution yields signal parameters ω_s, Ω_s, and ϕ_s retrieved simultaneously from a single evolution. Probing the Landau-Zener transition structure in this manner subverts the conventional assumption in quantum sensing that the resonant frequency ω_s must be known *a priori*, or carefully determined, for sensitive measurement of amplitude.

We realize the protocol on ultracold rubidium-87 atoms in the $F = 1$ hyperfine ground state. The ensemble of 1.8×10^6 atoms at 1.0 μK is approximately spherical with diameter 70 μm, held in a crossed optical dipole trap. A static $\hat{z}$ bias field yields Zeeman splitting by $\omega_L = 2\pi \times 603.5$ kHz, with all atoms initially in the $F = 1, m_F = -1$ state. We cancel the quadratic Zeeman shift of 53.5 Hz to well below 1 Hz with the ac Zeeman shift of a microwave field detuned from the clock transition by 387 kHz, so that the Zeeman triplet is symmetrically split. The atomic density is sufficiently low that spin-mixing dynamics do not affect the transverse spin magnitude [28] appreciably during the sweep. With dephasing and interaction effects nulled, spin projections follow single-atom spin-$\frac{1}{2}$ dynamics for at least 1 s [25]. A resonant rf field ($\Delta_c \approx 0$) along $\hat{x}$ creates dressed states $|\pm_1\rangle$ split by $\Omega_c(t)$ tunable from 4 kHz to 50 kHz. At low amplitudes, detuning errors $\Delta_c(t)$ generate increasingly large fluctuations in the splitting while at high amplitudes, Bloch-Siegert shifts require compensation. We add a test signal with weak amplitude Ω_s at frequency ω_s to our bias along $\hat{z}$. This is the sinusoidal signal we will attempt to measure.

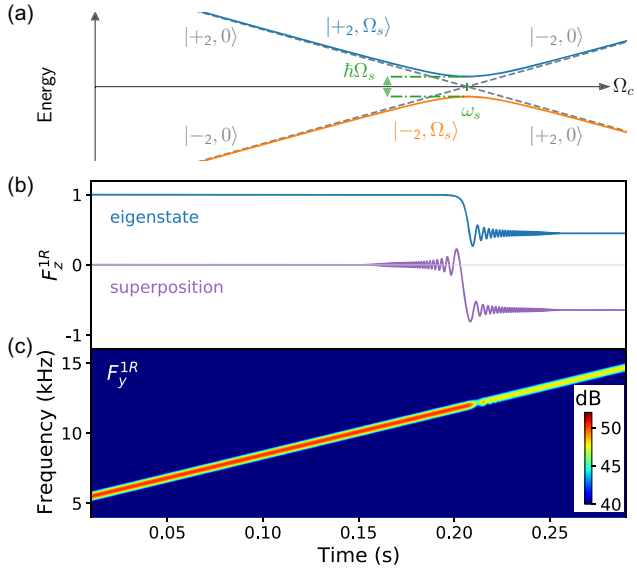

FIG. 1. Nonadiabatic sensing: under a sweep of sensing frequency $\Omega_c(t)$ the location of, and gap between, adiabatic eigenstates $|\pm_2, \Omega_s\rangle$ in an avoided crossing (a) reveal frequency ω_s and amplitude Ω_s, respectively, of a sinusoidal signal coupling the bare states $|\pm_2, 0\rangle$. Evolving spin projections [simulated, longitudinal (b), and transverse (c)] in the diabatic basis also encode signal parameters, but now as transition time, oscillations, and asymptotic value, which all depend (b) on the initial state. Transverse spin projection, shown as a spectrogram (c) for an initial superposition, oscillates at $\Omega_c(t)$ except near resonance where an avoided crossing emerges. A successful estimator robustly decodes signal parameters from measured spin projections.

We record a time series of the transverse spin projection with a minimally destructive Faraday spin-light interface, tuned to the magic-zero wavelength of 790.03 nm and with photodetected power of 6 mW spatially mode-matched to the atoms [25]. Digitized at 5 MSa/s, the spin projection is measured at the photon standard quantum limit (SQL). Over the 300 ms measurement time, scattering of probe photons depletes the atom number by ~20% and to account for this, we estimate the instantaneous total spin by a Hilbert transform method in a passband centered on ω_L. Normalized by this amplitude, the Faraday measurement is proportional to the transverse spin projection per atom.

This laboratory-frame measurement alternately probes the two transverse spin projections F_x^1 and F_y^1 of the first rotating frame as they precess past the laser propagation axis. The Faraday measurement, along an axis making angle ϕ_c with the $\hat{x}$ axis, is a quadrature-amplitude modulated signal $F_c^0 = F_x^1 \cos(\omega_c t + \phi_c) + F_y^1 \sin(\omega_c t + \phi_c)$, with carrier frequency ω_c and in-phase and quadrature amplitudes F_x^1 and F_y^1, respectively. Numerical demodulation with complex local oscillator $\exp[i(\omega_c t + \phi_c)]$ parallels the shift to the first interaction picture, where the resulting frame-1 measurement is a complex baseband signal proportional to $F_x^1 + iF_y^1$. In the sensing qubit frame 1R, this is $F_z^{1R} + iF_y^{1R}$: a continuous measurement of both the longitudinal, and one transverse, spin component of the evolving dressed state. See Supplemental Materials Sec. II for further processing detail [29].

Much of the subtlety of quantum metrology lies in how we infer the measurand from the quantum measurement record. While inferring a Rabi frequency from measurements of Rabi flopping is routine, we now face the much more challenging inverse problem of inferring the Rabi frequency and radiation frequency of the weak signal from the Landau-Zener evolution of the spin. An ungainly analytic solution exists in terms of sums of products of parabolic cylinder functions [48], however, their Stokes structure appears to impede regression, and no analytic solution is known for multifrequency signals.

Our solution was to retrieve signal parameters Ω_s, ω_s, and ϕ_s by parameter estimation on the underlying system of coupled ordinary differential equations. Such parameter estimation is well established for time-independent Hamiltonians [49], however, for time-dependent evolution prior demonstrations employed repeated evolutions with varying time-independent control [50], varying initial state [51], or dependence on preceding measurements [52]. Seeking a retrieval from a single unitary evolution, we regressed the numerical solution of the time-dependent Bloch equations to the data. We repeatedly solve the Bloch equations $\dot{\vec{F}}^{1R} = \vec{F}^{1R} \times \vec{\Omega}^{1R}$, where $\vec{F}^{1R} = F_x^{1R}\hat{x} + F_y^{1R}\hat{y} + F_z^{1R}\hat{z}$ is the Bloch vector and $\vec{\Omega}^{1R} = 2\Omega_s \cos(\omega_s t + \phi_s)\hat{x} + \Omega_c(t)\hat{z}$ the Rabi vector, varying the signal parameters and computing the cost function as the ℓ^2-norm of the residual between F_z^{1R} predicted by the Bloch solver [53], and the data. Working in frame-1R admits direct extension to retrieving multiple sinusoids, but the cost function is highly oscillatory and finding the global minimum is challenging, even with only three parameters [54]. Solving the Bloch equations is exactly equivalent to solving the time-dependent Schrödinger equation for $\hat{H}_{1R}(t)$, but is faster and obviates calculating expectation values.

While the retrieval uses only longitudinal spin data, successful estimation of parameters should result in the model agreeing with data in all three spin projections. Seeking to remove inessential dynamics independently of any particular solution, we transform to a spin-rotating frame-2S that corotates at the swept control Rabi frequency $\Omega_c(t)$ via $\hat{S}_{2S} = \exp(i\int_0^t \Omega_c(\tau)d\tau\hat{\sigma}_z/2) = \exp[(i\Omega_i t/2 + i\lambda t^2/4)\hat{\sigma}_z]$, as in Majorana's celebrated solution [58,59]. Without making a RWA, the Hamiltonian becomes $\hat{H}_{2S} = \hbar\Omega_s \cos(\omega_s t + \phi_s)[\cos(\Omega_i t + \lambda t^2/2)\hat{\sigma}_x - \sin(\Omega_i t + \lambda t^2/2)\hat{\sigma}_y]$, which interestingly is multiplicative with the signal and a prospect for development of the inverse problem. After making the RWA, only low-frequency dynamics remain, and the trajectories take a compact and elegant form related to the Cornu spiral [60], unwinding towards resonance and curling again beyond [61].

We generate projections in this frame through further demodulation of the transverse spin projection F_y^{1R} with the swept complex carrier $\exp[i(\Omega_i + \lambda t/2)t + i\phi_{2S}(t)]$, yielding F_y^{2S} and $-F_x^{2S}$ as the real and imaginary components. These transverse frame-2S projections prove useful for improving retrieval precision via analysis of the spin azimuthal phase $\phi_{2S}(t) = \text{atan2}(F_y^{2S}, F_x^{2S})$, with residual slow winding of ϕ_{2S} attributable to small errors in $\Omega_c(t)$. By fitting a smooth spline to the spin azimuth we can correct slow drifts in the Rabi control frequency, while leaving intact the small but rapid change in phase near resonance. While the optimizer considers only the longitudinal spin projection, these corrections enter the Bloch equations through $\Omega_c(t)$, improving both the accuracy of the solution and its presentation in frame-2S. As $\hat{S}_{2S}$ commutes with $\hat{\sigma}_z$, the longitudinal spin projection is unchanged: $F_z^{2S} = F_z^{1R}$. This yields all three projections in this frame and so represents continuous state tomography of the time-evolving system by double demodulation. In this context, subsequent parameter retrieval under our protocol represents sensing by process tomography of an ineluctably time-dependent quantum process. We now present a signal retrieval and its visualization on the Bloch sphere in frame-2S.

The sensor is initialized in a superposition of dressed eigenstates $(|+_{1R}\rangle + |-_{1R}\rangle)/\sqrt{2}$, equivalent to the lab-frame eigenstate $|+_0\rangle$. Rabi coupling is introduced, immediately commencing an upward sweep in amplitude from $\Omega_c = 2\pi \times 7$ kHz to 13 kHz over 300 ms. In the absence of a test signal, the adiabatic theorem indicates the amplitudes of the dressed states remain unchanged even as their splitting steadily increases. We introduce a weak test signal at $\omega_s = 2\pi \times 10$ kHz, which drives a Landau-Zener transition evident in Fig. 2(a) (colored trace). Optimization in frame-1R converges after order 10^4 iterations [Fig. 2(a), black trace], yielding a multiparameter estimate of $B_s = \Omega_s/\gamma = 3.34(2)$ nT for signal amplitude and $\omega_s = 2\pi \times 10.004\,34(16)$ kHz for signal frequency. In fact, the digitally synthesized sweep proceeds in steps of 3 Hz, likely accounting for much of the frequency estimate residual (see Supplemental Material, Sec. I [29]).

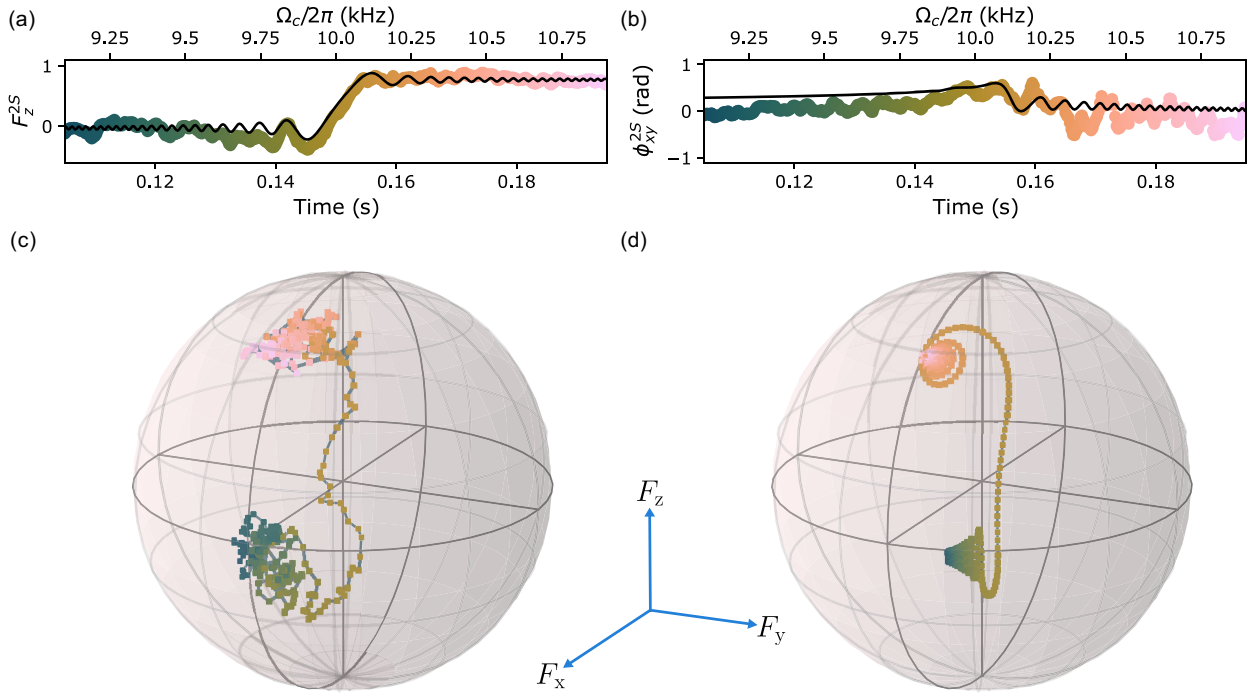

FIG. 2. Fitting a quantum process model to a continuous measurement of unitary evolution estimates frequency and amplitude in a single shot. Time series for (a) longitudinal spin projection and (b) equatorial spin angle show the continuous measurement (color) and the model (black) retrieving precision parameter estimates of $B_s = 3.34(2)$ nT, $\omega_s = 2\pi \times 10.004\,34(16)$ kHz and $\phi_s = 3.93(14)$ rad. Evolution as Bloch sphere trajectories for smoothed data (c) and model (d) in frame-2S, with the same color mapping for time [63].

Figure 2 shows data (c) and model (d) as trajectories on the Bloch sphere in frame-2S, with the common color code denoting time. With only longitudinal data used in parameter estimation, strong correlation between data and estimated solution of not only the longitudinal projection but of the full state evolution instills confidence parameter estimation has succeeded. A calibration shot with constant requested $\Omega_c = 2\pi \times 10$ kHz yielded an *unswept* Rabi parameter estimate [64] of $B_s = 3.272(9)$ nT, covarying significantly with the control error in Ω_c the estimate of which varies by order Ω_s between calibration shots. This inadvertently revealed an inherent advantage in swept multiparameter estimation: while the resonance crossing may be shifted by such detuning error, the amplitude estimate remains almost entirely unaffected, making the swept sensor considerably more robust.

As with the Rabi protocol, the initial state determines whether the Landau-Zener protocol is sensitive to phase. Measurements beginning with an initial superposition depend on the phase difference at resonance crossing. It is well known that such phase-sensitive measurements have the highest possible (linear) sensitivity to radiation in quadrature [17], while being completely insensitive to radiation in phase with the qubit. In contrast, the Rabi protocol beginning in an eigenstate is phase insensitive, measuring purely amplitude, but at the price of being only quadratically sensitive to it.

Our measurement presented in Fig. 2 commenced with a superposition and thus should be phase sensitive. The retrieved signal phase $\phi_s = 3.93(14)$ rad was, however, not repeatable which we attribute to the residual error in Ω_c—even after the spline interpolation correction—integrated up over the $2\pi \times 3000$ radian sweep prior to resonance. Repeatable amplitude retrieval despite this demonstrates a fundamental advantage of the Landau-Zener sensor: even for a signal exactly in phase at resonance, where a Rabi measurement would have zero sensitivity, the Landau-Zener time series shows a characteristic transient providing frequency and amplitude information. Further, this suggests that amplitude and phase can be separately and unambiguously measured with linear sensitivity in a single initialization. We have also performed phase-insensitive retrieval of signal parameters commencing in a dressed eigenstate, retrieving frequency and amplitude without including a phase parameter.

Our retrieval variances correspond to amplitude sensitivity of 11 pT/$\sqrt{\text{Hz}}$, frequency sensitivity of 0.026 Hz/Hz$^{3/2}$, and phase sensitivity of 0.084 rad/$\sqrt{\text{Hz}}$. In general, the sensitivities appear to be nonlinear functions of sweep rate λ, sweep time, initial state, Faraday probe SNR, and each other. Some insight follows from considering $\sqrt{\lambda}$, a critical frequency in swept-sine spectrum analyzers: in classical analyzers it defines the minimum undistorted resolution bandwidth (RBW) and hence spectral resolution [2]. In the quantum analyzer, $\sqrt{\lambda}$ is the adiabaticity threshold for *amplitude*: for weak signals $\Omega_s < \sqrt{\lambda}$, the transition full-width approaches $\sqrt{\lambda/\pi}$ rather than Ω_s [59,65]. In this limit

the quantum analyzer should equal the frequency resolution of its classical counterpart. Our sweeps of 6 kHz/300 ms are equivalent to RBW $(\sqrt{\lambda/\pi})/2 = 100$ Hz, and so resolve 60 channels across the span. On average 6×10^3 atoms scatter probe photons during the 5 ms channel transit [25], giving a prospective atom SQL of 0.99 pT/$\sqrt{\text{Hz}}$. Furthermore, under unitary evolution all time points after the transition are affected, implying a lower detection limit than this simple transit-time model predicts.

A single-spin nanoscale analyzer [17] using Qdyne methods to retrieve single-tone signal parameters in a 1.5 MHz band around a fixed 1.51 GHz resonance was 74 dB less sensitive than our swept resonance analyzer, which uses 63 dB more spins. Frequency and phase sensitivities were almost identical. Sweeping the resonance not only covers octaves of bandwidth but also obviates the dynamic range constraints of Rabi aliasing.

Finally, we have not considered the quantum backaction of the continuous measurement. Simultaneous Faraday measurements of two spin quadratures furnished by Larmor precession yield planar spin squeezed states [66], and it is plausible that analogous nondemolition backaction may enhance dressed-state spectral sensing.

The linearly swept qubit is an archetypal problem of time-dependent quantum mechanics, and the Landau-Zener solution thereof emerges naturally in quantum measurement of signals with frequency unknown. We have used this insight to demonstrate a Landau-Zener multiparameter estimator for frequency, amplitude, and phase, operating on a single unitary evolution. The long coherence time of radio-frequency-dressed cold atoms enables a quantum spectrum analyzer achieving time-bandwidth product of 1800, amplitude precision of 20 pT, and sub-Hertz resolution in frequency. We have retrieved rich spectra from multitone signals, with encouraging resolution of component frequencies, although so far without precision estimation of amplitudes [29]; we are optimistic that precision retrievals of rich spectra are possible. We envision applications including compact very-low-frequency (VLF) receivers, and microscale nuclear magnetic resonance (NMR) spectroscopy in Earth's field. More fundamentally, the analyzer heralds a new class of intrinsically time-dependent sensing protocols, neither Ramsey nor Rabi, which harness nonadiabaticity for quantum measurement.

We thank Russell Anderson, Michael Barson, James Saunderson, and Alexander Wood for helpful discussions, the anonymous referees for valuable comments which improved the manuscript, and James Pollock and Maeva Berchon for assistance in preparing the apparatus. This work was supported by an Australian Government Research Training Program scholarship, and funded by the Australian Research Council under Linkage Project No. LP200100082.

*christopher.bounds@monash.edu

[1] C. L. Degen, F. Reinhard, and P. Cappellaro, Quantum sensing, Rev. Mod. Phys. **89**, 035002 (2017).
[2] M. Engelson, *Modern Spectrum Analyzer Theory and Applications* (Artech House, Dedham, 1984).
[3] W. Koenig, H. K. Dunn, and L. Y. Lacy, The sound spectrograph, J. Acoust. Soc. Am. **18**, 19 (1946).
[4] W. Thomson, IV. Harmonic analyzer, Proc. R. Soc. **27**, 371 (1878).
[5] A. A. Michelson and S. W. Stratton, A new harmonic analyzer, Am. J. Sci. **s4-5**, 1 (1898).
[6] S. Kotler, N. Akerman, Y. Glickman, and R. Ozeri, Nonlinear single-spin spectrum analyzer, Phys. Rev. Lett. **110**, 110503 (2013).
[7] M. Chipaux, L. Toraille, C. Larat, L. Morvan, S. Pezzagna, J. Meijer, and T. Debuisschert, Wide bandwidth instantaneous radio frequency spectrum analyzer based on nitrogen vacancy centers in diamond, Appl. Phys. Lett. **107**, 233502 (2015).
[8] S. Magaletti, L. Mayer, J.-F. Roch, and T. Debuisschert, A quantum radio frequency signal analyzer based on nitrogen vacancy centers in diamond, Commun. Eng. **1**, 1 (2022).
[9] U. Haeberlen and J. S. Waugh, Coherent averaging effects in magnetic resonance, Phys. Rev. **175**, 453 (1968).
[10] P. Facchi, D. A. Lidar, and S. Pascazio, Unification of dynamical decoupling and the quantum Zeno effect, Phys. Rev. A **69**, 032314 (2004).
[11] J.-M. Cai, B. Naydenov, R. Pfeiffer, L. P. McGuinness, K. D. Jahnke, F. Jelezko, M. B. Plenio, and A. Retzker, Robust dynamical decoupling with concatenated continuous driving, New J. Phys. **14**, 113023 (2012).
[12] A. Ajoy, Y.-X. Liu, K. Saha, L. Marseglia, J.-C. Jaskula, U. Bissbort, and P. Cappellaro, Quantum interpolation for high-resolution sensing, Proc. Natl. Acad. Sci. U.S.A. **114**, 2149 (2017).
[13] S. Schmitt, T. Gefen, F. M. Stürner, T. Unden, G. Wolff, C. Müller, J. Scheuer, B. Naydenov, M. Markham, S. Pezzagna, J. Meijer, I. Schwarz, M. Plenio, A. Retzker, L. P. McGuinness, and F. Jelezko, Submillihertz magnetic spectroscopy performed with a nanoscale quantum sensor, Science **356**, 832 (2017).
[14] J. M. Boss, K. S. Cujia, J. Zopes, and C. L. Degen, Quantum sensing with arbitrary frequency resolution, Science **356**, 837 (2017).
[15] D. Trypogeorgos, A. Valdés-Curiel, N. Lundblad, and I. B. Spielman, Synthetic clock transitions via continuous dynamical decoupling, Phys. Rev. A **97**, 013407 (2018).
[16] R. P. Anderson, M. J. Kewming, and L. D. Turner, Continuously observing a dynamically decoupled spin-1 quantum gas, Phys. Rev. A **97**, 013408 (2018).
[17] N. Staudenmaier, S. Schmitt, L. P. McGuinness, and F. Jelezko, Phase-sensitive quantum spectroscopy with high-frequency resolution, Phys. Rev. A **104**, L020602 (2021).
[18] J. Meinel, V. Vorobyov, B. Yavkin, D. Dasari, H. Sumiya, S. Onoda, J. Isoya, and J. Wrachtrup, Heterodyne sensing of microwaves with a quantum sensor, Nat. Commun. **12**, 2737 (2021).
[19] K. Khodjasteh and L. Viola, Dynamically error-corrected gates for universal quantum computation, Phys. Rev. Lett. **102**, 080501 (2009).

[20] M. Ban, Photon-echo technique for reducing the decoherence of a quantum bit, J. Mod. Opt. **45**, 2315 (1998).
[21] J. M. Taylor, P. Cappellaro, L. Childress, L. Jiang, D. Budker, P. R. Hemmer, A. Yacoby, R. Walsworth, and M. D. Lukin, High-sensitivity diamond magnetometer with nanoscale resolution, Nat. Phys. **4**, 810 (2008).
[22] S. Kotler, N. Akerman, Y. Glickman, A. Keselman, and R. Ozeri, Single-ion quantum lock-in amplifier, Nature (London) **473**, 61 (2011).
[23] V. M. Frey, S. Mavadia, L. M. Norris, W. de Ferranti, D. Lucarelli, L. Viola, and M. J. Biercuk, Application of optimal band-limited control protocols to quantum noise sensing, Nat. Commun. **8**, 2189 (2017).
[24] H. Zhang, K. Arai, C. Belthangady, J.-C. Jaskula, and R. L. Walsworth, Selective addressing of solid-state spins at the nanoscale via magnetic resonance frequency encoding, npj Quantum Inf. **3**, 31 (2017).
[25] M. Jasperse, M. J. Kewming, S. N. Fischer, P. Pakkiam, R. P. Anderson, and L. D. Turner, Continuous Faraday measurement of spin precession without light shifts, Phys. Rev. A **96**, 063402 (2017).
[26] O. V. Ivakhnenko, S. N. Shevchenko, and F. Nori, Nonadiabatic Landau–Zener–Stückelberg–Majorana transitions, dynamics, and interference, Phys. Rep. **995**, 1 (2023).
[27] A. Silberfarb, P. S. Jessen, and I. H. Deutsch, Quantum state reconstruction via continuous measurement, Phys. Rev. Lett. **95**, 030402 (2005).
[28] Y. Liu, S. Jung, S. E. Maxwell, L. D. Turner, E. Tiesinga, and P. D. Lett, Quantum phase transitions and continuous observation of spinor dynamics in an antiferromagnetic condensate, Phys. Rev. Lett. **102**, 125301 (2009).
[29] See Supplemental Material at http://link.aps.org/supplemental/10.1103/PhysRevLett.132.093401 for (I) Detailed breakdown of apparatus, (II) Data processing, (III) Analysis procedure, (IV) Signal calibration, (V) Preliminary multi-tone measurements, and (VI) Avenues for multiparameter estimation development, which includes Refs. [30–47].
[30] H. A. M. Taylor, C. C. Bounds, A. Tritt, and L. D. Turner, Unambiguous measurement in an unshielded microscale magnetometer with sensitivity below 1 pT/rHz, arxiv:2309.11825.
[31] P. T. Starkey, C. J. Billington, S. P. Johnstone, M. Jasperse, K. Helmerson, L. D. Turner, and R. P. Anderson, A scripted control system for autonomous hardware-timed experiments, Rev. Sci. Instrum. **84**, 085111 (2013).
[32] D. Hilbert, *Grundzüge einer allgemeinen theorie der linearen integralgleichungen* (Leipzig, B. G. Teubner, 1912).
[33] S. Kornblith *et al.*, JuliaDSP/DSP.jl: v0.7.8, Zenodo (2022), 10.5281/zenodo.7406426.
[34] Abraham. Savitzky and M. J. E. Golay, Smoothing and differentiation of data by simplified least squares procedures, Anal. Chem. **36**, 1627 (1964).
[35] P. Dierckx, *Curve and Surface Fitting with Splines* (Clarendon Press, Oxford, 1995).
[36] M. F. Ahmad, N. A. M. Isa, W. H. Lim, and K. M. Ang, Differential evolution: A recent review based on state-of-the-art works, Alex. Eng. J. **61**, 3831 (2022).
[37] C. T. Kelley, *4. The BFGS Method, in Iterative Methods for Optimization*, Frontiers in Applied Mathematics and Statistics (SIAM, Philadelphia, 1999), pp. 71–86.
[38] A. Tritt, J. Morris, J. Hochstetter, R. P. Anderson, J. Saunderson, and L. D. Turner, Spinsim: A GPU optimized python package for simulating spin-half and spin-one quantum systems, Comput. Phys. Commun. **287**, 108701 (2023).
[39] Y. Ma, V. Dixit, M. Innes, X. Guo, and C. Rackauckas, A Comparison of automatic differentiation and continuous sensitivity analysis for derivatives of differential equation solutions, arxiv:1812.01892.
[40] I. Dattner, A model-based initial guess for estimating parameters in systems of ordinary differential equations, Biometrics **71**, 1176 (2015).
[41] O. Aydogmus and A. H. Tor, A modified multiple shooting algorithm for parameter estimation in ODEs using adjoint sensitivity analysis, Appl. Math. Comput. **390**, 125644 (2021).
[42] R. T. Q. Chen, Y. Rubanova, J. Bettencourt, and D. K. Duvenaud, Neural ordinary differential equations, in *Advances in Neural Information Processing Systems* (Curran Associates, Inc., Red Hook, 2018), Vol. 31.
[43] E. M. Turan and J. Jäschke, Multiple shooting for training neural differential equations on time series, IEEE Cont. Syst. Lett. **6**, 1897 (2022).
[44] J. Q. Davis, K. Choromanski, J. Varley, H. Lee, J.-J. Slotine, V. Likhosterov, A. Weller, A. Makadia, and V. Sindhwani, Time dependence in non-autonomous neural ODEs, arxiv:2005.01906.
[45] S. Blanes, F. Casas, J. A. Oteo, and J. Ros, The Magnus expansion and some of its applications, Phys. Rep. **470**, 151 (2009).
[46] A. Arnal, F. Casas, C. Chiralt, and J. A. Oteo, A unifying framework for perturbative exponential factorizations, Math. Mag. **9**, 637 (2021).
[47] F. Bloch, Nuclear induction, Phys. Rev. **70**, 460 (1946).
[48] N. V. Vitanov and B. M. Garraway, Landau-Zener model: Effects of finite coupling duration, Phys. Rev. A **53**, 4288 (1996).
[49] J. Zhang and M. Sarovar, Quantum Hamiltonian identification from measurement time traces, Phys. Rev. Lett. **113**, 080401 (2014).
[50] L. E. de Clercq, R. Oswald, C. Flühmann, B. Keitch, D. Kienzler, H.-Y. Lo, M. Marinelli, D. Nadlinger, V. Negnevitsky, and J. P. Home, Estimation of a general time-dependent Hamiltonian for a single qubit, Nat. Commun. **7**, 11218 (2016).
[51] K. Siva, G. Koolstra, J. Steinmetz, W. P. Livingston, D. Das, L. Chen, J. M. Kreikebaum, N. J. Stevenson, C. Jünger, D. I. Santiago, I. Siddiqi, and A. N. Jordan, Time-dependent Hamiltonian reconstruction using continuous weak measurements, PRX Quantum **4**, 040324 (2023).
[52] M. Naghiloo, A. N. Jordan, and K. W. Murch, Achieving optimal quantum acceleration of frequency estimation using adaptive coherent control, Phys. Rev. Lett. **119**, 180801 (2017).
[53] Ch. Tsitouras, Runge–Kutta pairs of order 5(4) satisfying only the first column simplifying assumption, Comput. Math. Appl. **62**, 770 (2011).

[54] We use the DifferentialEquations.jl ecosystem [55] to identify the correct basin with a global optimizer [56] before a fast local optimizer [55,57] locates the minimum and extracts parameter covariances. The global optimizer is constrained only by requiring ω_s within the span, and positive Ω_s less than a nominal maximum well into the adiabatic regime. See Supplemental Material [29] Sec. III.

[55] C. Rackauckas and Q. Nie, DifferentialEquations.jl–a performant and feature-rich ecosystem for solving differential equations in JULIA, J. Open Res. Software **5**, 15 (2017).

[56] R. Feldt, BlackBoxOptim.jl, GitHub Repository, https://github.com/robertfeldt/BlackBoxOptim.jl (2018).

[57] P. K. Mogensen and A. N. Riseth, OPTIM: A mathematical optimization package for Julia, J. Open Source Software **3**, 615 (2018).

[58] E. Majorana, Atomi orientati in campo magnetico variabile, Nuovo Cimento **9**, 43 (1932).

[59] P. O. Kofman, O. V. Ivakhnenko, S. N. Shevchenko, and F. Nori, Majorana's approach to nonadiabatic transitions validates the adiabatic-impulse approximation, Sci. Rep. **13**, 5053 (2023).

[60] F. Zhuang, J. Zeng, S. E. Economou, and E. Barnes, Noise-resistant Landau-Zener sweeps from geometrical curves, Quantum **6**, 639 (2022).

[61] For a weak signal and evolving from an initial eigenstate, the Cornu spiral appears eidetically in orthographic projection with one focus centered on the pole; kinematically a large Bloch sphere rolls without slipping on the planar spiral [62].

[62] A. G. Rojo and A. M. Bloch, The rolling sphere, the quantum spin, and a simple view of the Landau–Zener problem, Am. J. Phys. **78**, 1014 (2010).

[63] F. Crameri, G. E. Shephard, and P. J. Heron, The misuse of colour in science communication, Nat. Commun. **11**, 5444 (2020).

[64] S. J. White, C. C. Bounds, H. Taylor, A. Tritt, and L. D. Turner (unpublished).

[65] N. V. Vitanov, Transition times in the Landau-Zener model, Phys. Rev. A **59**, 988 (1999).

[66] G. Colangelo, F. M. Ciurana, L. C. Bianchet, R. J. Sewell, and M. W. Mitchell, Simultaneous tracking of spin angle and amplitude beyond classical limits, Nature (London) **543**, 525 (2017).